Composites: Part A 43 (2012) 158–164

Contents lists available at SciVerse ScienceDirect

Composites: Part A

journal homepage: www.elsevier.com/locate/compositesa

Moisture absorption of unidirectional hybrid composites

E. Barjasteh *, S.R. Nutt

Department of Chemical Engineering and Materials Science, University of Southern California, Los Angeles, CA 90089, United States

ARTICLE INFO

Article history:
Received 8 June 2011
Received in revised form 5 October 2011
Accepted 7 October 2011
Available online 14 October 2011

Keywords:
A. Hybrid
A. Polymer-matrix composites
B. Environmental degradation

ABSTRACT

Unidirectional hybrid composite rods were conditioned in humid air to investigate the sorption kinetics and the effects of moisture on mechanical and physical properties. Sorption curves were obtained for both hybrid and non-hybrid composite rods to determine characteristic parameters, including the diffusion coefficient (D) and the maximum moisture uptake (M_∞). The moisture uptake for the hybrid composites generally exhibited Fickian behavior (no hybridization effects), behaving much like non-hybrid composites. A two-dimensional diffusion model was employed to calculate moisture diffusivities in the longitudinal direction. Interfaces and thermally-induced residual stresses affected the moisture diffusion. In addition, the effect of hygrothermal aging on glass transition temperature (T_g), short beam shear strength (SBS), and tensile strength was determined for hygrothermal exposure at 60 °C and 85% relative humidity (RH). Property retention and reversibility of property degradation were also measured. Microscopic inspection revealed no evidence of damage.

1. Introduction

New applications of fiber-reinforced polymer composites (FRPCs) are arising in non-traditional sectors of industry, such as civil infrastructure, automotive, and power distribution. For example, composites are being used in place of steel to support high-voltage overhead conductors. In this application, conductive strands of aluminum are wrapped around a solid composite rod comprised of unidirectional carbon and glass fibers in an epoxy matrix [1]. Composite-core conductors such as these are expected to eventually replace conventional steel-reinforced conductors because of the reduced sag at high temperatures, lower weight, higher ampacity, and reduced line losses [2,3].

Resistance to environmental attack and the long-term retention of properties are major issues that could potentially prevent the widespread acceptance of composite conductors. Conductors during service are typically exposed to moisture and temperatures that eventually can degrade the mechanical properties and lead to premature failure [4,5]. Therefore, understanding the kinetics and mechanisms of degradation during hygrothermal exposure is essential to establish safe limits on service conditions, necessary inspection/replacement frequency, and for design of appropriate protective measures.

Hygrothermal effects on composite properties have been reported for carbon-fiber (CF) and glass-fiber (GF)-epoxy composites exposed to humid air or submerged in hot water [4,6,7]. The moisture uptake for these materials indicated Fickian diffusion behavior in some cases, while in others, non-Fickian behavior was reported [8–12]. While these reports documented the effects of hygrothermal exposure on CF and GF composites, few investigations have focused on the effects of such exposure on hybrid or unidirectional composites [5,13–15].

The purpose of this work was to evaluate the moisture absorption behavior and associated mechanical degradation of unidirectional hybrid composites designed to support overhead conductors. The mechanism of moisture behavior of the hybrid composites was also compared with single-fiber reinforced (non-hybrid) composites, and the radial and longitudinal diffusivities were calculated using the Fickian law. The mechanical and physical properties were measured after different exposure times to evaluate property retention, and samples were dehydrated to determine the extent to which properties could be recovered.

2. Experimental procedure

2.1. Materials

Fig. 1 shows the cross-section of the unidirectional hybrid composite rod used in this study. The rod was 7.75 mm in diameter, and consisted of an inner core of carbon fiber (CF), an outer shell of glass fiber (GF), and an anhydride-cured epoxy (proprietary formulation). The hybrid composite rods (H) were manufactured via pultrusion (Composite Technology Corporation, Irvine, CA) yielding an overall fiber volume fraction of ~67%.

* Corresponding author. Tel.: +1 4086052785.
E-mail address: Barjaste@usc.edu (E. Barjasteh).

1359-835X/$ - see front matter © 2011 Elsevier Ltd. All rights reserved.
doi:10.1016/j.compositesa.2011.10.003

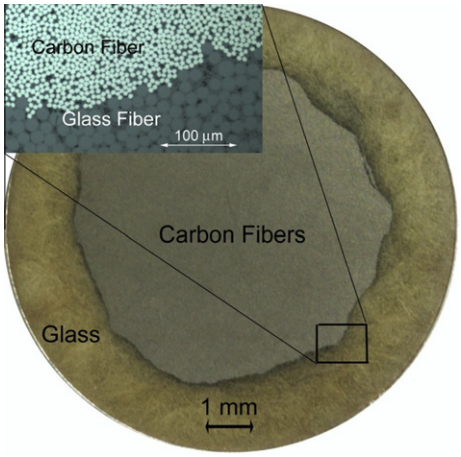

Fig. 1. Cross-section of unidirectional CF/GF hybrid composite rod, showing the CF core region, surrounded by the GF shell [7]. (For interpretation of the references to colour in this figure legend, the reader is referred to the web version of this article.)

2.2. Conditioning

The specimens for the water sorption study were cut to lengths of 48 mm and divided into two groups, end-capped and uncapped. Specimens in the first group were capped on both ends using a silicone sealant to restrict the moisture sorption to the radial direction (assuming uniform diffusion in the radial direction). Note that when conductors are attached to lattice towers in service, the composite ends are placed in aluminum fixtures (dead-ends and connectors). Specimens in the second group were not capped, permitting water sorption in the *z*- and *r*-directions simultaneously.

Fig. 2 shows the weight loss of specimens exposed to air at 60 °C and 100 °C as a function of exposure time, illustrating the dryness of specimens prior to hygrothermal exposure. The weight loss was nearly 0.11% for the first 2 days of exposure, which was attributed primarily to removal of moisture and low-molecular-weight species. An additional 14 days of drying caused an additional 0.01% weight loss, which was attributed to matrix degradation (mainly a dehydration reaction) and removal of sizing. The weight loss within the first 2 days of exposure at 60 °C was less than the loss at 100 °C (see Fig. 2), a result of the lower activation energy for moisture diffusion and low-molecular-weight species. Thus, 2 days of drying prior to hygrothermal exposure was sufficient to remove nearly all of the absorbed moisture resulting from exposure, and this drying period was adopted to prevent further thermal degradation. Note

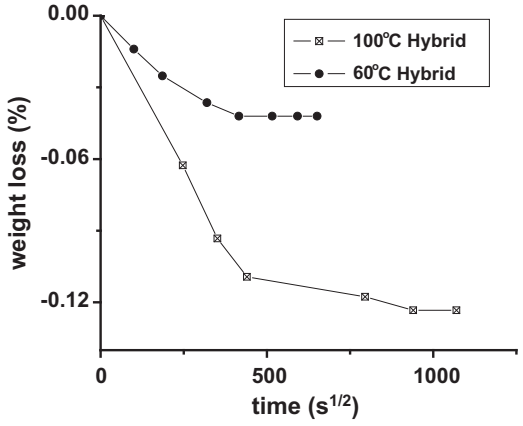

Fig. 2. Weight change of the specimens as the function of exposure time at 100 °C and 60 °C.

that no thermal degradation occurred after 2 days of exposure at 60 °C (identical to the moisture exposure temperature).

Specimens for water sorption measurements and for mechanical and thermal testing were conditioned in an environmental chamber set to conditions of 60 °C and 85% relative humidity (TPS T30RC-2 and Hotpack 435304). Specimens were periodically removed from the environmental chamber to measure weight change using an analytical balance with 0.01 mg accuracy (ACCULAB LA-60). The specimens were also removed periodically to conduct thermal and mechanical tests in the *wet* and *dry* states (achieved by drying for 3 days at 100 °C). Dried specimens were evaluated to determine the extent of reversibility in properties after moisture absorption experiments. Prior to weighing, all specimens were surface-dried to remove residual surface water. The weight change was calculated according to:

$$\frac{W_w - W_o}{W_o} \times 100\% \tag{1}$$

where W_w is the wet weight, and W_o is the dry weight.

2.3. Short beam shear strength, tensile strength, thermal stability and inspection

Short beam shear strength (SBS) and tensile strength measurements were performed to determine the effects of hygrothermal exposure. For SBS measurements, specimens were cut to 66.5 mm, while tensile samples were cutto 106.7 mm. SBS was measured at room temperature in accordance with ASTM D4475-02 using a load frame (INSTRON 5567) and a bend fixture with a span length six times the diameter and a crosshead displacement rate of 1.3 mm/min. Tensile strength was measured using a universal testing machine (INSTRON 5585) at room temperature in accordance to ASTM D3916-02. The initial values of SBS and tensile strengths were 46 MPa and 2280 MPa.

The change in glass transition temperature (T_g) with exposure time was determined by dynamic mechanical analysis (DMA, TA Instruments DMA2980) with a dual cantilever beam clamp. Sample beams 60 × 9.5 × 1.6 mm were cut from the CF core of the rod. A load frequency of 1 Hz was imposed over a temperature range of 25–250 °C, and T_g was determined from the peak of loss modulus curve.

Transverse and longitudinal sections of the exposed samples were cut and polished using a broad-beam ion polisher (JEOL SM-09010). Ion polishing (~5.2 kV and ~110 mA) resulted in sections free of relief, preserving the exposed layer. Light microscopy (Olympus Vanox) and scanning electron microscopy (SEM; JSM 7001F) were used to examine the polished sections.

2.4. Calculation of 1D and 2D moisture diffusion

Capping specimens ensured that moisture diffused only in the radial direction. The amount of moisture diffusing in time *t*, M_t, can be expressed as follows [16]:

$$\frac{M_t}{M_\infty} = 1 - \sum_{n=1}^{\infty} \frac{4}{R^2 \alpha_n^2} \exp(-\alpha_n^2 D t) \tag{2}$$

where M_∞ is the saturation level of water absorption, D_r is the radial diffusion coefficient, R is the radius, and α_n is the n_{th} root of the zero-order Bessel function. Note that the effects of CF core/GF shell interface on the moisture diffusion are assumed to be negligible, and diffusion along fiber–matrix interfaces is neglected. In addition, the D_r is the average diffusivity over locations, calculated from the best fit of Eq. (2) to experimental data.

Uncapped rods allow for moisture diffusion both axially (through the rod ends) and radially during humidity exposure

tests. The moisture sorption behavior can be predicted by the two-dimensional diffusion equation in cylindrical coordinates, as shown in Eq. (3) below. In addition, moisture diffusion through the ends is the combination of longitudinal diffusion through the CF core and the GF shell, with different diffusion coefficients, D_{CZ} and D_{GZ}, respectively.

$$\frac{\partial C}{\partial t} = (V_{GF}D_{GZ} + V_{CF}D_{CZ})\frac{\partial^2 C}{\partial Z^2} + D_r \frac{1}{r}\frac{\partial}{\partial r}\left(r\frac{\partial C}{\partial r}\right) \tag{3}$$

where V_{CF} and V_{GF} are the volume fractions of CF-core and GF-shell sections, respectively, and D_r is the radial moisture diffusion. (Note that a single radial diffusion coefficient was used to simplify the analysis). The initial moisture concentration at any r and Z within the specimens assumed to be zero. Assuming $2L$ is the length and R is the outer radius of the specimen, the boundary conditions at z- and r-directions are:

$$C = C_0 \quad \text{at} \quad r = R \quad \text{and} \quad Z = \pm L \tag{4}$$

where C_0 is the concentration of moisture in humid air. The solution of Eq. (3) is obtained by separation of variables to solve the two-dimensional partial differential equation, and is shown in Eq. (5) below.

$$\frac{C(r,z,t)}{C_\infty} = 1 - \frac{8}{\pi R}\sum_{n=0}^{\infty}\sum_{m=1}^{\infty}\frac{J_0(\alpha_m r)}{(2n+1)\alpha_m \cdot J_1(\alpha_n r)} \cdot \sin\left[\frac{(2n+1)\pi(z+L)}{2L}\right] \cdot \exp\left[-\left(\alpha_m^2 + \frac{2(n+1)^2\pi^2}{4\left(\frac{D_r}{D_z}L\right)^2}\right)D_r t\right] \tag{5}$$

Here C_∞ is the moisture concentration at equilibrium, and J_0 and J_1 are the zero- and first-order Bessel functions of the first kind, respectively, and α_m is the m_{th} root of the zero-order Bessel function. The amount of diffusing moisture within the specimen is given by the integral,

$$M_t = \int_0^R 2\pi r dr \cdot \int_{-L}^{L} C(r,z,t)\cdot dz \tag{6}$$

which yields Eq. (7):

$$\frac{M_t}{M_\infty} = 1 - \frac{32}{\pi^2}\sum_{n=0}^{\infty}\frac{1}{(\alpha_m R)^2}\cdot\exp[-\alpha_m^2 D_r t]\cdot\sum_{m=0}^{\infty}\frac{1}{(2n+1)^2} \cdot \exp\left[-\frac{(2n+1)^2\pi^2}{\left(4\left(\frac{D_r}{v_{CF}D_{cz}+v_{GF}D_{GZ}}\right)L\right)^2}D_r t\right] \tag{7}$$

where M_∞ is the maximum amount of moisture at equilibrium.

3. Results and discussion

3.1. Weight change

Fig. 3 shows the weight change as a function of time for capped and uncapped hybrid composites exposed to 60 °C/85% RH. The percent weight gain is plotted as a function of the square root of the exposure time ($s^{1/2}$). Each data point represents the average of three measurements on individual specimens, and the error bars show standard deviation values. The moisture uptake increased with increasing exposure time for all specimens, eventually reaching saturation. However, the saturation level for uncapped specimens (~1%) was greater than for capped specimens (~0.5%). In addition, for any exposure time, the amount of absorbed moisture

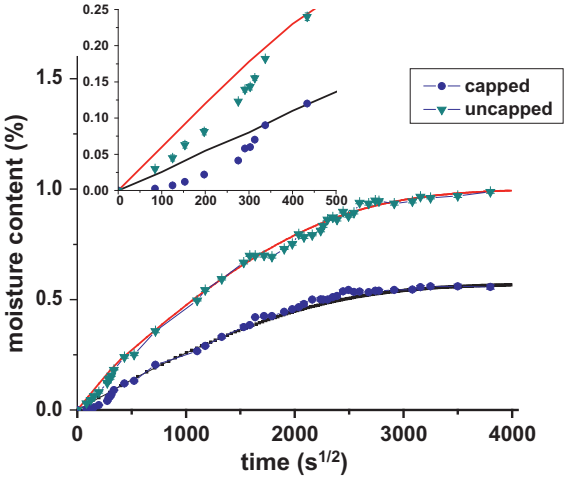

Fig. 3. Weight change versus the square root of time ($s^{1/2}$) for composite rods exposed to 60 °C and 85% humidity chamber for capped and uncapped specimens. (For interpretation of the references to colour in this figure legend, the reader is referred to the web version of this article.)

for the uncapped specimens was greater than that of capped specimens, a result of simultaneous longitudinal and radial diffusion.

The Fickian nature of moisture absorption for both capped and uncapped specimens is shown in Fig. 3. The solid lines superimposed on the data points, represent fits for theoretical Fickian curves. For short exposure times, the Fickian curves deviated from the measured data for both capped and uncapped specimens, as shown in Fig. 3 (top left). The weight loss curves were slightly sigmoidal in shape, and deviated from Fickian behavior for short exposure times [16].The best fit to the data from the later stage of the sorption curve (neglecting initial stage data) was used to calculate diffusivity, because the sigmoidal behavior observed in early stages did not yield accurate diffusivity values.

Similar non-Fickian behavior was reported for highly cross-linked epoxy, and was attributed to changes in resin properties during moisture sorption, particularly diffusivity, and hence retardation in moisture uptake [9,17]. However, the mechanism of short-time non-Fickian moisture absorption remains unclear, largely due to the complexity of the process. In this study, the deviation from Fickian behavior was negligible except for a brief initial period, and the data generally conformed to ideal behavior. Thus the non-ideal behavior was attributed to a transient surface concentration (no instantaneous surface equilibrium occurred) [8].

Table 1 shows the moisture diffusivities within the capped and uncapped hybrid specimens. In capped specimens, diffusion occurred only in the radial direction, and the D value was calculated by a nonlinear fit of the diffusion equation (Eq. (2)) to data points. For calculations, the first five terms ($n = 5$) of summation in Eq. (2) were taken into consideration. (The variation of results by considering 6 terms instead of 5 was negligible, ~0.02%). Note that in service, moisture diffusion in rods is primarily one-dimensional (radial) diffusion, similar to the capped specimens.

In uncapped specimens, moisture diffused in both radial and longitudinal directions (from the unsealed ends). The longitudinal

Table 1
Radial and longitudinal moisture diffusivities and maximum moisture uptake for the glass, carbon, and hybrid composite specimens.

	Hybrid	Carbon	Glass
D_r (m^2/s)	7.5×10^{-13}	8.3×10^{-13}	6.3×10^{-13}
D_z (m^2/s)	3.5×10^{-12}	4.0×10^{-12}	1.8×10^{-12}
$M_{\infty,\text{capped}}$ (%)	0.45	0.6	0.4
$M_{\infty,\text{uncapped}}$ (%)	1	1.2	0.75

diffusivity was calculated by a fit of the derived equation for two-dimensional diffusion (Eq. (7)) to experimental results. To calculate D_z, we assumed that D_r was identical to the value calculated for the capped specimens. In addition, the theoretical longitudinal diffusion, D_z, was identical to a linear combination of CF-core and CF-shell longitudinal diffusivities.

$$D_z = V_{CF}D_{cz} + V_{CF}D_{cz} \tag{8}$$

The longitudinal diffusivity for the hybrid composite ($D_z = 3.5 \times 10^{-12}$) was four times greater than the radial diffusivity ($D_r = 7.5 \times 10^{-13}$), confirming that the rate of longitudinal diffusion along the fiber/matrix interface was much greater than diffusion in the radial direction. The lower radial diffusivity is attributed to the more tortuous diffusion pathways in radial directions. The additional (longitudinal) diffusion pathway available in uncapped specimens accounted for the greater rate of weight gain and the increased maximum moisture uptake.

To investigate the effect of hybridization of glass with carbon fibers, additional moisture absorption experiments were performed on all-CF/epoxy and all-GF/epoxy rods. Note that all specimens (hybrid and non-hybrid) had fiber loadings of ~67%. Fig. 4 shows the sorption curve for the uncapped GF/epoxy, CF/epoxy, and GF/CF/epoxy hybrid (H) composites. The moisture absorption data for the GF and CF specimens followed a typical Fickian curve, similar to the H specimen, indicating that hybridization did not influence the moisture absorption behavior. However, the CF/epoxy showed greater moisture uptake (1.2%) than the H specimen (1%), while the GF/epoxy specimens showed lower moisture uptake (0.75%). Similar trends were observed for diffusivity coefficients.

The diffusivities of the G and C specimens (both capped and uncapped) were calculated using Eqs. (2) and (7), respectively, and the results are shown in Table 1. As noted, the diffusivity coefficients for the C specimens were the greatest (particularly the longitudinal diffusivity), while those for the G specimens were the lowest. The greater diffusivity for the C specimens was attributed in part to the smaller fiber diameters (~7 μm) compared to glass fibers (~20 μm), which resulted in greater interface area per unit volume (nearly three times greater for equivalent fiber loadings). Note that scaling the diffusion coefficients with fiber areas resulted in similar non-dimensional values, supporting the assertion that the greater interface area was responsible for the greater diffusivity of the C specimens. In addition, the fiber and matrix are often

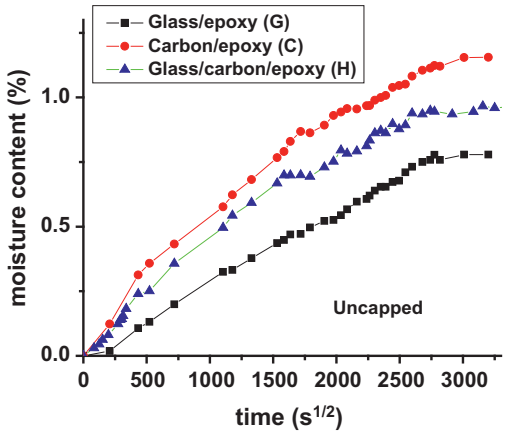

Fig. 4. Percent weight change versus the square root of time for uncapped unidirectional glass/carbon/epoxy (H), carbon/epoxy (C), and glass/epoxy (G) composite rods exposed to 60 °C and 85% humidity chamber. (For interpretation of the references to colour in this figure legend, the reader is referred to the web version of this article.)

imperfectly bonded, and micro-void channels along interfaces are not uncommon, resulting in free space which provides a pathway for accelerated diffusivity [18].

The diffusivity and maximum moisture uptake (saturation level) can be affected by the state of stress in the matrix. For example, a tensile stress produces a volumetric strain in the matrix, which increases moisture diffusion, while compression stresses show opposite effects on diffusion [19–21]. In the present case, the manufacturing process causes residual stress in the rods. During pultrusion, the epoxy is thermally cured in the die (~240 °C). During cooling, thermal stresses arise from the mismatch in coefficients of thermal expansion (CTE) of the components, as shown in Table 2 [22,23]. As the matrix attempts to contract during cooling, the carbon fiber remains resists dimensional changes (nearly zero CTE), causing axial tension in the matrix. Associated stresses at the fiber–matrix interface can increase moisture diffusion, diffusivity, and maximum moisture uptake.

The longitudinal diffusivity in the hybrid specimens (calculated from curve fits) was greater than values calculated from the classical formula (Eq. (8)). Eq. (8) was used to calculate D_z for the hybrid composite, using the individual diffusivities of carbon/epoxy and glass/epoxy composites. Note that the CF core and the GF shell each comprised nearly 50% of the transverse cross-sectional area, and Eq. (8) does not account for interface effects. Thus, the calculated value for D_z was 2.9×10^{-12} m^2/s. However, the value for D_z calculated from the best fit to sorption data was 3.5×10^{-12} m^2/s, indicating an increase in diffusivity associated with the GF shell/CF core interface. The increased diffusivity was attributed to stress concentration arising from the CTE mismatch between the CF core and the GF shell (see Table 2) [23].

3.2. Microstructure and damage

Polished sections of the hybrid specimens aged for different exposure times (before and after saturation) were inspected to determine types of damage, such as fiber/matrix interfacial debonding and matrix cracking. Fig. 5 shows a glass-fiber section of an ion-polished specimen after 3500 s$^{0.5}$of exposure. Even after saturation (above ~2500$t^{0.5}$), no interfacial debonding was observed. Like the unexposed specimen, the surface of the aged specimen remained smooth, but with slight discoloration.

3.3. Thermal and mechanical properties

Prolonged hygrothermal aging effects are often manifested by changes in thermal and mechanical properties. Degradation of composite properties results from physical aging (matrix swelling and plasticization) and chemical aging that accompanies moisture absorption. However, fiber-dominated mechanical properties, particularly for unidirectional composites, are generally unaffected even after long-term exposures, barring degradation of large portions of the matrix. This study focused on changes in the SBS strength, T_g, and tensile strength with increasing hygrothermal exposure time.

3.3.1. Glass-transition temperature (T_g)

The maximum service temperature of polymeric composites is typically related to the value of T_g for the matrix [24]. Therefore, changes in T_g due to exposure in hygrothermal environments influence design considerations. Fig. 6a shows the T_g of the capped and uncapped specimens as a function of aging times up to 16 weeks (above saturation). Note that the T_g values were determined from the peak of the loss modulus curve. The T_g values decreased by 15 °C with increasing aging time for all specimens, and nearly identical results were observed for the capped and uncapped specimens. A significant loss in T_g occurred prior to saturation (nearly

Table 2
Coefficients of thermal expansion for individual components in composite rods.

	Epoxy	Glass fiber	Carbon fiber	Epoxy/glass	Epoxy/carbon
CTE_{axial} (10^{-6}/°C)	60	4.9	−0.7	6.56	−0.35

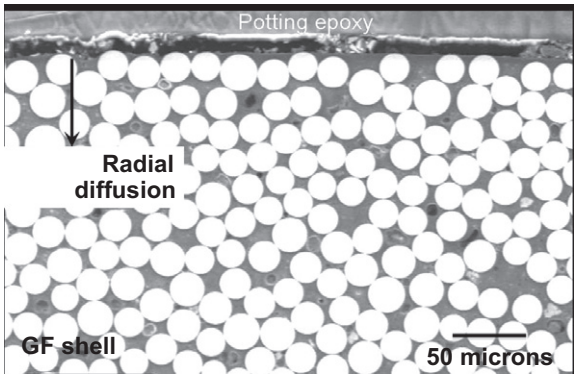

Fig. 5. SEM micrograph of a specimen exposed to 60 °C and 85% relative humidity after nearly 5 months.

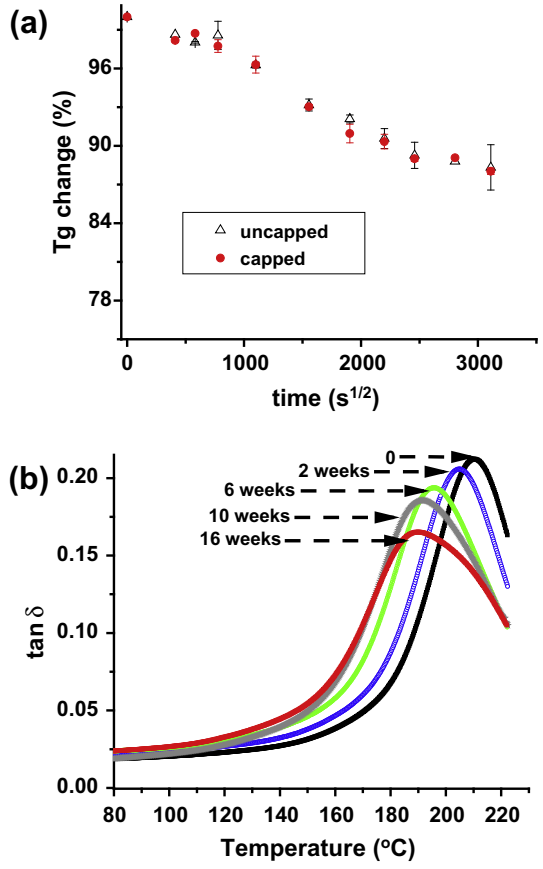

Fig. 6. (a) Percent change in glass transition temperature versus the square root of time for the capped and uncapped hybrid specimens exposed at 60 °C and 85% relative humidity for nearly 4 months. (b) Change in loss tangent as a function of temperature and time for uncapped specimen. (For interpretation of the references to colour in this figure legend, the reader is referred to the web version of this article.)

13 °C), while the rate of reduction in T_g decreased as the saturation point was approached. The observed decrease in T_g was related to the diffusion of water molecules into the composite matrix that disrupted Van der Waals and hydrogen bonds in the epoxy, resulting in increased chain mobility [25]. For uncapped specimens, the longitudinal moisture diffusion was limited to specimen ends (the bulk of the specimen remained nearly intact), resulting in an identical T_g change for the capped specimens.

Moisture uptake can change the viscoelastic properties of the matrix, resulting in changes in the location, shape, and height of the loss tangent obtained from DMA [15,26–28]. Fig. 6b shows changes in loss tangent data as a function of exposure time and temperature. Note that the values between 25 °C and 80 °C were omitted for clarity, but they were approximately constant. Increasing the exposure time caused the tan δ peak to shift to lower temperatures, corresponding to a decrease in T_g for the hybrid composite. Meanwhile, the height of the loss tangent peak decreased with increasing aging time (nearly 8% decrease after 16 weeks), reflecting increasing matrix plasticization during moisture uptake [15]. In addition, the glass transition region for the aged specimen broadened with respect to the un-aged specimen, as shown in Fig. 6b. Such broadening stems from non-uniform moisture distribution associated with the presence of voids within the specimen (shown in Fig. 5). Water infiltration into voids reportedly can lead to local variations in T_g [26].

3.3.2. Shear properties

Long-term hygrothermal exposure caused changes in the short beam shear (SBS) strength of the composite rods. Fig. 7 shows the SBS strength as a function of exposure time for capped and uncapped rods aged at 60 °C and 85% relative humidity. For both types of rods, the SBS strength decreased by nearly 14%. Thus, for both capped and uncapped specimens, similar decreasing trends were observed in T_g and SBS strength values (as shown in Figs. 6a and 7), indicating matrix degradation.

Degradation of the in-plane shear strength of polymer composites can result from deterioration of interfacial bonding, matrix cracking, plasticization, and chemical aging of the matrix (e.g. hydrolysis) [29,30]. During moisture uptake, micro-cracking frequently occurs after the saturation level is reached, causing non-Fickian behavior, water infiltration, and deviation of weight gain data from M_∞. The Fickian behavior of the hybrid composite (Fig. 1) along with the polished sections (Fig. 5) indicates that no micro-cracking and interface de-bonding occurred. Thus, the observed decrease in SBS strength was attributed primarily to matrix plasticization, as explained in Section 3.3.1.

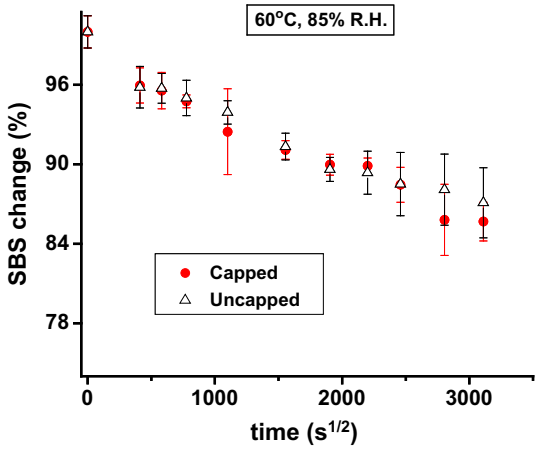

Fig. 7. Change in SBS strength of the capped and uncapped composite rods exposed at 60 °C and 85% relative humidity for nearly 4 months. (For interpretation of the references to colour in this figure legend, the reader is referred to the web version of this article.)

3.3.3. Recovery of T_g and SBS strength

The extent of recovery of the T_g and SBS strength after hygrothermal exposure was investigated to determine the reversibility of loss in properties. Specimens were pre-exposed to moisture for 16 weeks, then dried for 2 days at100 °C to remove absorbed moisture. For the capped specimen, the wet/dry percentages of SBS and T_g were 86/91 and 88/89, respectively, while the percentages for the uncapped specimen were 87/92 and 88/88, respectively. Stated differently, for capped and uncapped specimens, the recovery of SBS strength after drying was 91–92%, while the recovery in T_g was 88–89%. The partial recovery of these properties (2–4%) was attributed to permanent degradation of the matrix and/or the fiber/matrix interface. The diffused water partially bonded with polar groups such as hydroxyls through hydrogen bonding or reacted with the epoxy or hardener. These water molecules did not diffuse out during specimen drying, resulting in microstructural degradation and permanent loss of properties [31,32].

3.3.4. Tensile properties

Tensile strength (TS) is a major design consideration for high voltage electrical conductors because of stress arising from self-weight, thermal fluctuations, ice, and wind. Hygrothermal exposure can alter the tensile strength of composites over time, which in turn can affect long-term durability of conductors in service. Fig. 8 shows the change in tensile strength of hybrid composites exposed at 60 °C and 85% R.H. for nearly 100 days. A decrease of almost 6.0% was observed after 100 days of exposure, while a decrease of ~5.5% in strength occurred before saturation (72 days). The tensile strength was unchanged after saturation, indicating negligible further degradation. Note that the TS values of the exposed specimens were greater than the rated tensile strength (RTS (a conservative estimate of conductor overall strength calculated by multiplying by a derating factor) [33], shown as a dashed line in Fig. 8) of the composite rod (nearly 94.5% of the TS of the unaged specimen) up to the saturation time. The strength of the composite samples used in this study was nearly 6% greater than the RTS.

Matrix plasticization and swelling during hygrothermal exposure caused reduction in fiber/matrix interfacial strength, reducing the load transfer ability and thus tensile strength. In capped specimens, only a small amount of moisture was absorbed during hygrothermal aging, hence reducing the effect of moisture on tensile strength [32]. Thus, because tensile strength is a fiber-dominated property and fibers are largely unaffected by hygrothermal aging, the longitudinal tensile-strength retention was greater than the retention of SBS and T_g for the same exposure time. As a result, the 5% drop in tensile strength was attributed to matrix plasticization and loss of interfacial strength.

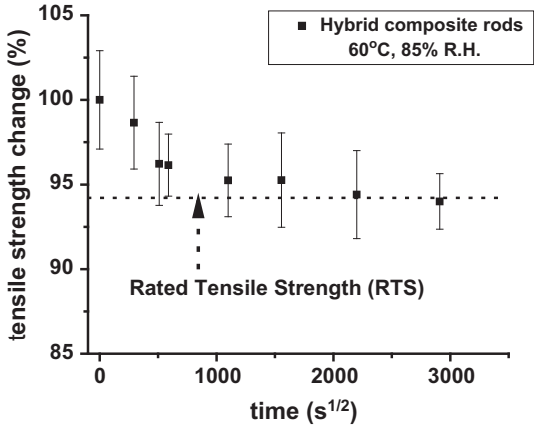

Fig. 8. Percent change in tensile strength of the composite rods exposed at 60 °C and 85% relative humidity for nearly 4 months.

4. Conclusions

The effect of moisture absorption on the mechanical and thermal properties of hybrid composite rods designed to support overhead transmission lines was investigated. The hybrid composite exhibited Fickian moisture absorption behavior, much like the all-CF and all-GF composites. However, the presence of the CF-GF interface in the hybrid composite changed the moisture diffusivity. In particular, longitudinal diffusivity in the hybrid composite increased due to the presence of GF/CF interfaces. Furthermore, the smaller CF diameters provided greater interface area per unit volume (compared to the GF shell), and thus more possible pathways for rapid diffusion, which accelerated the diffusion process.

Thermal and mechanical testing after long-term moisture exposure provided insights into the property retention of the hybrid composite rods. Moderate losses in short beam shear (SBS), tensile strength and glass transition temperature (T_g) with aging time were observed, a portion of which amounted to permanent moisture-induced damage. Note that the tensile strength values (a key design parameter) exceeded the rated tensile strength up to the saturation point. In addition, weight change did not provide a useful indicator of property degradation, as the present study demonstrated that weight change was only weakly correlated with the losses in T_g and mechanical properties.

Residual thermal stresses that arise during the manufacture of pultruded composites result from thermal mismatch between fiber and matrix and from matrix shrinkage during cure. Such residual stresses enhance moisture diffusivity and uptake during hygrothermal exposure, which in turn contributes to property degradation. Thermally induced stresses place the matrix under tension, accelerating diffusion, particularly within the carbon fiber core, where the fiber CTE is near-zero. Furthermore, the hybrid structure gives rise to a region of stress concentration at the CF-GF boundary that could lead to enhanced longitudinal and hoop diffusion. These regions are likely to weaken progressively during moisture uptake, adversely affecting the mechanical properties of the hybrid composite rod. Therefore, measures to reduce the residual internal stress, either by changes to the rod design or to manufacturing protocols, may be needed to increase the resistance of such hybrid composites to hygrothermal exposure.

Acknowledgements

The authors acknowledge Nikhil Kar, Roy Tsai, and Zhong Chen for their assistance and support, and Composite Technology Corporation for supplying test samples.

References

[1] Alawar A, Bosze EJ, Nutt SR. A composite core conductor for low sag at high temperatures. IEEE Trans Power Delivery 2005;20(3):2193–9.
[2] Bosze EJ, Alawar A, Bertschger O, Tsai YI, Nutt SR. High-temperature strength and storage modulus in unidirectional hybrid composites. Compos Sci Technol 2006;66(13):1963–9.
[3] Alawar A, Bosze EJ, Nutt SR. A hybrid numerical method to calculate the sag of composite conductors. Electr Power Syst Res 2006;76(5):389–94.
[4] Ellyin F, Maser R. Environmental effects on the mechanical properties of glass-fiber epoxy composite tubular specimens. Compos Sci Technol 2004;64:1863–74 [Compendex].
[5] Paciornik S, Martinho FM, de Mauricio MHP, d'Almeida JRM. Analysis of the mechanical behavior and characterization of pultruded glass fiber-resin matrix composites. Compos Sci Technol 2003;63:295–304 [Compendex].
[6] Ke L, Bao W, Chen L, Wong YS, Tam NFY. Effects of humic acid on solubility and biodegradation of polycyclic aromatic hydrocarbons in liquid media and mangrove sediment slurries. Chemosphere 2009;76:1102–8 [Compendex].

[7] Tsai YI, Bosze EJ, Barjasteh E, Nutt SR. Influence of hygrothermal environment on thermal and mechanical properties of carbon fiber/fiberglass hybrid composites. Compos Sci Technol 2009;69(3-4):432–7.
[8] De Wilde WP, Shopov PJ. A simple model for moisture sorption in epoxies with sigmoidal and two-stage sorption effects. Compos Struct 1994;27:243–52 [Copyright 1994, IEE].
[9] Crank J. A theoretical investigation of the influence of molecular relaxation and internal stress on diffusion in polymers. J Polym Sci 1953;11(2):151–68.
[10] Xiao GZ, Shanahan MER. Swelling of DGEBA/DDA epoxy resin during hydrothermal aging. Polymer 1998;39:3253–60 [Compendex].
[11] Xiao GZ, Shanahan MER. Water absorption and desorption in an epoxy resin with degradation. J Polym Sci Part B (Polym Phys) 1997;35:2659–70 [Copyright 1997, IEE].
[12] Xiao GZ, Delamar M, Shanahan MER. Irreversible interactions between water and DGEBA/DDA epoxy resin during hygrothermal aging. J Appl Polym Sci 1997;65:449–58 [Compendex].
[13] Botelho EC, Pardini LC, Rezende MC. Hygrothermal effects on damping behavior of metal/glass fiber/epoxy hybrid composites. Mater Sci Eng A 2005;399:190–8 [Compendex].
[14] Ishai O, Hiel C, Luft M. Long-term hygrothermal effects on damage tolerance of hybrid composite sandwich panels. Composites 1995;26:47–55 [Compendex].
[15] Karbhari VM, Xian G. Hygrothermal effects on high VF pultruded unidirectional carbon/epoxy composites: Moisture uptake. Composites Part B 2009;40:41–9 [Compendex].
[16] Rank JC. The mathematics of diffusion. Oxford University Press; 1956.
[17] Springer GS, editor. Environmental effects on composite materials. Lancaster, PA, USA: Technomic Publ Co; 1984.
[18] Tsenoglou CJ, Pavlidou S, Papaspyrides CD. Evaluation of interfacial relaxation due to water absorption in fiber-polymer composites. Compos Sci Technol 2006;66(15):2855–64.
[19] Wan YZ, Wang YL, Huang Y, He BM, Han KY. Hygrothermal aging behaviour of VARTMed three-dimensional braided carbon–epoxy composites under external stresses. Compos Part A – Appl Sci Manuf 2005;36(8):1102–9.
[20] Neumann S, Marom G. Stress dependence of the coefficient of moisture diffusion in composite materials. Polym Compos 1985;6:9–12 [Copyright 1985, IEE].
[21] Weitsman Y. Stress assisted diffusion in elastic and viscoelastic materials. J Mech Phys Solids 1987;35:73–93 [Copyright 1987, IEE].
[22] Burks B, Armentrout DL, Kumosa M. Failure prediction analysis of an ACCC conductor subjected to thermal and mechanical stresses. IEEE Trans Dielectr Electr Insul 2010;17:588–96 [Compendex].
[23] Kar N HY, Barjasteh E, Nutt SR. Tension-tension fatigue of hybrid composite rods. Compos Part A: Appl Sci Manuf 2011.
[24] Jankowsky JL, Wong DG, DiBerardino MF, Cochran RC. Evaluation of upper use temperature of toughened epoxy composites. In: Proceedings of the symposium on assignment of the glass transition, March 4, 1993 – March 5, 1993; 1994; Atlanta, GA, USA: ASTM; 1994. p. 277–92.
[25] Zhou J, Lucas JP. Hygrothermal effects of epoxy resin. Part I: the nature of water in epoxy. Polymer 1999;40:5505–12 [Compendex].
[26] Khan LA, Nesbitt A, Day RJ. Hygrothermal degradation of 977-2A carbon/epoxy composite laminates cured in autoclave and Quickstep. Composites Part A 2010;41:942–53 [Copyright 2011, The Institution of Engineering and Technology].
[27] Nogueira P, Ramirez C, Torres A, Abad MJ, Cano J, Lopez J, et al. Effect of water sorption on the structure and mechanical properties of an epoxy resin system. J Appl Polym Sci 2001;80:71–80 [Compendex].
[28] Xian G, Karbhari VM. DMTA based investigation of hygrothermal ageing of an epoxy system used in rehabilitation. J Appl Polym Sci 2007;104:1084–94 [Compendex].
[29] Komai K, Minoshima K, Shiroshita S. Hygrothermal degradation and fracture process of advanced fibre-reinforced plastics. Mater Sci Eng A 1991;A143:155–66 [Compendex].
[30] Kawagoe M, Hashimoto S, Nomiya M, Morita M, Qiu J, Mizuno W, et al. Effect of water absorption and desorption on the interfacial degradation in a model composite of an aramid fibre and unsaturated polyester evaluated by Raman and FT infra-red microspectroscopy. J Raman Spectrosc 1999;30:913–8 [Copyright 1999, IEE].
[31] Errajhi OAZ, Osborne JRF, Richardson MOW, Dhakal HN. Water absorption characteristics of aluminised E-glass fibre reinforced unsaturated polyester composites. Compos Struct 2005;71:333–6 [Copyright 2006, IEE].
[32] Taib RM, Ishak ZAM, Rozman HD, Glasser WG. Effect of moisture absorption on the tensile properties of steam-exploded Acacia mangium fiber-polypropylene composites. J Thermoplast Compos Mater 2006;19:475–89 [Copyright 2006, The Institution of Engineering and Technology].
[33] Orawski G, Henrioul G, Barbarito M, de Weck P, Ghannoum E, Gidlund JI, et al. Loading and strength of overhead transmission lines. Electra 1990:64–97 [Compendex].